Journal of Power Sources 224 (2013) 211–224

Contents lists available at SciVerse ScienceDirect

Journal of Power Sources

journal homepage: www.elsevier.com/locate/jpowsour

Modeling, validation and analysis of mechanical stress generation and dimension changes of a pouch type high power Li-ion battery

Rujian Fu*, Meng Xiao, Song-Yul Choe

Mechanical Engineering, Auburn University, 1418 Wiggins Hall, Auburn, AL 36830, USA

HIGHLIGHTS

- ► An electrochemical, thermal and mechanical model for Li ion battery is developed.
- ► The model is validated against experiment data.
- ► The battery thickness is a function of SOC.
- ► Stress in anode is higher than that in cathode particles.
- ► The highest stress is generated in the electrode particles near the separator.

ARTICLE INFO

Article history:
Received 26 June 2012
Received in revised form
21 September 2012
Accepted 23 September 2012
Available online 4 October 2012

Keywords:
Li ion polymer battery
Electrochemical
Thermal and mechanical model
Stress modeling
Volume change

ABSTRACT

Mechanical stress is generated in electrode particles of a Lithium ion Polymer Battery (LiPB) during charge and discharge. The stress can cause cracks and fractures in the solid particles over time when cells are cycled, which leads to a disorder and a fracture of the electrodes. In order to understand the mechanism, a stress model for a pouch type high power LiPB is developed based on electrochemical and thermal model, where the stress induced by the ion concentration in the electrode particles is considered. The stress in the particles causes changes in the electrode volumes and leads to changes in the thickness of a battery cell, which is measured using a device designed with two linear voltage displacement transducers (LVDT). This model is validated against experimental data obtained from a pouch cell. Analysis shows that the magnitude of stress depends upon locations and C rate, while the thickness of a single cell is mainly affected by the state of charge (SOC), but not C rate.

1. Introduction

LiPB is mostly preferred as an energy storage device in hybrid and electric vehicles because of its high power and energy density as well as its high columbic efficiency. However, the behavior of internal physical variables of a cell is not well known. Thus, there have been attempts to describe the battery mathematically using principles of electrochemical kinetics, potential theory, mass transports, energy balance and elasticity.

The first electrochemical model proposed by Doyle et al. [1] assumed that a cell is made of several thin-film layers. The working mechanism is described with electrochemical principles. Fuller et al. [2] extended the model by considering other cathode materials like $LiCoO_2$, $LiMn_2O_4$ and used this model to investigate the effects of material property parameters on the performance of a cell. After that, the model was included with transference number [3], activity coefficient in electrolyte [4], diffusion coefficient in $LiPF_6$ electrolyte [5], and particle size distributions on the discharge capacity [6].

On the other hand, the material property, related to ion transport and intercalation/de-intercalation mechanism, is strongly affected by heat generation and mechanical stress that take place at charging and discharging. This relationship is depicted in Fig. 1, where the electrochemical kinetics and mass transport are coupling with thermal and mechanical behaviors. Song [7] and Smith [8] improved the electrochemical model by adding the energy equations considering various heat generation terms. Chen and Evans [9] then included the behavior of heat transfer to the electrochemical model. The typical heat generations considered are from different sources including the entropy heating, the Joule heating and the heat of mixing.

In addition, mechanical stress is generally generated by change of ion concentration in particles, so that electrodes expands or

* Corresponding author. Tel.: +1 334 750 7274; fax: +1 334 844 3307.
E-mail address: rzf0007@auburn.edu (R. Fu).

0378-7753/$ – see front matter © 2012 Elsevier B.V. All rights reserved.
http://dx.doi.org/10.1016/j.jpowsour.2012.09.096

Nomenclature

A	plate area of cell (cm^2)
a_s	specific surface area of electrode (cm^{-1})
c_s	ion concentration in solid phase (mol L^{-1})
c_e	ion concentration in electrolyte (mol L^{-1})
C_{equi}	equivalent capacity of cell (A h)
C_p	heat capacity (J kg^{-1} K^{-1})
D	diffusion coefficient in electrode (cm^2 s^{-1})
E	Young's modulus (MPa)
E_{chem}	electrochemical energy (J)
F	Faraday's constant (96,487 C mol^{-1}) or force (N)
g	swelling coefficient
h	thickness of composite electrode mixed with electrolyte (cm)
h_{cell}	thickness of the single cell (cm)
h_c	convective heat transfer coefficient (W K^{-1})
I	current of the cell (A)
i_0	reference exchange current density (A cm^{-2})
J	flux of ion diffusion (mol cm^{-2} s^{-1})
j	transfer current density(A cm^{-3})
L	width of micro cell (cm)
l	circumference of the packaging material (cm)
N	number of micro cells in the single cell
m	mass of the single cell (kg)
n	amount of active electrode material (mol)
OCV	open circuit voltage (V)
P_{chem}	power contributing to the increase of chemical energy (W)
Q_{rev}	reversible heat generation rate (W)
Q_{irr}	irreversible heat generation rate (W)
Q_{convec}	heat convection rate (W)
R	universal gas constant (8.3143 J mol^{-1} K^{-1})
R_s	radius of spherical electrode particle (cm)
r	radius (cm)
SOC	state of charge
T	cell temperature (K)
T_∞	ambient temperature (K)
t	time (s)
U_{equi}	equilibrium potential (V)
u	radial displacement in electrode particle (cm)
V	volume of composite electrode mixed with electrolyte (cm^3)
V_T	terminal voltage of cell (V)
w	width of the single cell (cm)
x	stoichiometric number in anode or coordinate along the width of micro cell
x_1	coordinate along the width of single cell
x_2	coordinate along the thickness of single cell
y	stoichiometric number in cathode
t_+^0	initial transference number

Greek symbols

α	transfer coefficient for an electrode reaction
ε	strain or porosity of a porous medium
ε_r	radial strain in electrode particle
ε_s	volume fraction of solid phase in composite electrode
ε_t	tangential strain in electrode particle
ϕ_e	potential in electrolyte phase (V)
ϕ_s	potential in solid phase (V)
η	surface overpotential of electrode reaction(V)
κ	ionic conductivity of electrolyte (S cm^{-1})
κ_D	concentration driven diffusion conductivity (A cm^{-1})
ν	Poisson's ratio
ρ	density (g cm^{-3})
σ	stress (MPa) or conductivity of solid active material (S cm^{-1})
σ_r	radial stress in electrode particle (MPa)
σ_t	tangential stress in electrode particle (MPa)
σ_h	hydrostatic stress in electrode particle(MPa)
Ω	theoretical partial molar volume of Li-ion (cm^3 mol^{-1})
Ω_{fitted}	fitted partial molar volume of Li-ion based on experimental data (cm^3 mol^{-1})
ω	fractional expansivity of electrode material

Subscripts

cell	the single cell
e	electrolyte phase
max	maximum
pack	the packaging material
r	radial direction in electrode particle
s	solid phase
t	tangential direction in electrode particle
0	without expansion caused by lithiation or initial state
0%	0% state of charge
100%	100% state of charge
−	anode
+	cathode

Superscripts

eff	effective
Li	Lithium ion

contracts depending on charging and discharging. Fracture of the electrode materials is one of the durability issues, which is caused by ion-induced stress. During the diffusion process, inhomogeneous distribution of Li-ions in an electrode particle causes inhomogeneous localized volume expansions, which induces mechanical stress. When stress exceeds certain limits, the electrode would experience material failure, associated with cracking or fracture.

There have been several attempts to investigate the mechanism of stress generation and volume expansion using models. Christensen and Newman [10,11] first proposed a detailed model based on theories of transport and elasticity to predict stress in a single anode particle and a cathode particle. They found that high power application of Li-ion battery has an increased likelihood of particle fracture, but reducing the size of particles can help to prevent such failure.

Another alternative method to describe the stress induced by the concentration gradient of solutes is proposed by Prussin [12], who first applied this method to describe stress generation during the inclusion of boron and phosphorus into silicon water. Yang [13] followed the same method and modeled chemical stress of solute in a thin plate. In 2007, Zhang [14] first applied this method to analyze the stress in a Li ion battery. Similar to thermal stress, a model for stress generation in a single cathode particle was proposed and the simulation result showed similar predictions as those in Christensen and Newman's work [11]. Zhang [15] then extended the model under a consideration of heat generation for ellipsoidal particles, and concluded that larger aspect ratios are

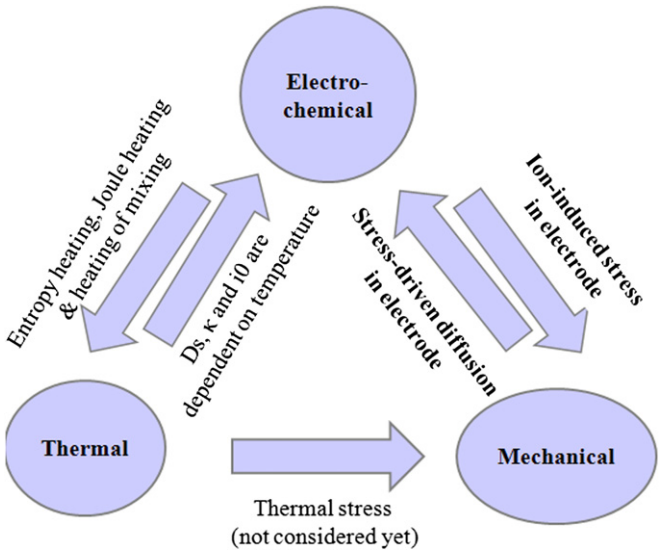

Fig. 1. Principle diagram for electrochemical–thermal–mechanical effects.

preferred over spherical particles for better cell performance. Based on similar elastic equations, Harris et al. [16] extended the case for electrode particles with presence of small internal cracks and pores. They found that stress generation also depends largely on the internal microstructure of particles other than the material properties of electrode.

Instead of modeling single particles only, other authors studied the effects of stress generation on composite electrodes mixed with electrolyte. Garcia [17] proposed a model for stress generation in composite electrode under consideration of different arrangements of particles. Golmon [18] applied the composite electrode theory to develop a model for electrochemical–mechanical behavior in macro and micro scales.

In addition, some other authors have proposed models that include stress generation and electrochemical behavior in a cell. Bower [19] predicted variations of stress, electrochemical reactions and diffusion in a one dimensional half cell. Christensen [20] incorporated calculations of stress generation in particles to a cell-sandwich model and considered nonlinear lattice expansion in anode material.

The mechanical response (stress generation and volume expansion) also has effects on electrochemical behavior, as shown in Fig. 1. The most important effect is stress (pressure)-driven diffusion. J.C.M. Li [21] first analyzed the effect of stress on chemical potential based on the partial molar volume of solute. X. Zhang [14,15] then applied this theory in Li ion electrode particles and analyzed the effect of stress on diffusion. So far, most researchers [10,14,18,20] have found that stress-driven diffusion could decrease the gradient of ion concentration and stress generation in electrode, but has little effect on the terminal voltage of a cell [20]. There are other ways that mechanical response could affect electrochemical behavior. Gomadam [22] investigated the effect of volume changes of particles on the change of porosity. Bower [19] modified the Nernst equation by considering the rest potential as a function of stress.

However, all the predictions above have not coupled with the electrochemical thermal models of LiPB or compared with experiments. We developed a coupled model that considers the electrochemical, thermal and the mechanical elastic principle and is validated against the experimental data obtained for a high power pouch cell, including the terminal voltage, current, temperature and change of battery thickness under multiple cycles.

2. Setup for modeling

The pouch type of single cell to be investigated has a chemistry of $LiMn_2O_4$/Carbon for the electrodes. Its geometry is shown at the right side of Fig. 2. The single cell has a dimension of 164 mm × 250 mm × 5 mm with 15.7 A h capacity. It is assumed that the single cell is composed of multiple micro cells that are connected in parallel by current collectors. The schematic diagram of a micro cell is shown at the left side of Fig. 2. The micro cell is mathematically described by a one dimensional sandwiched model, which is composed of a composite anode mixed with electrolyte, a separator and a composite cathode mixed with electrolyte. The electrode materials are porous. When the cell is charged or discharged, electrons go through external circuit while ions are transported in the electrode and electrolyte. Chemical reactions take place at the surface of electrode particles that contact with electrolyte, followed by ion diffusions inside the electrode particles. Three heat source terms are considered in this model: change of entropy, Joule heating and heat of mixing.

Non-uniform distribution of ions inside an electrode particle can cause inhomogeneous localized volume changes which induce mechanical stress. In certain region of an electrode particle as highlighted in Fig. 3, the increase of Li^+ concentration results in strains in radial and tangential directions and causes localized volume expansion. Since the neighboring material does not necessarily have the same amount of increase in Li^+ concentration, it tends to resist the highlighted volume from expansion and therefore, mechanical stress is induced. The electrode particles are approximated as spheres with the same radius. It is assumed that

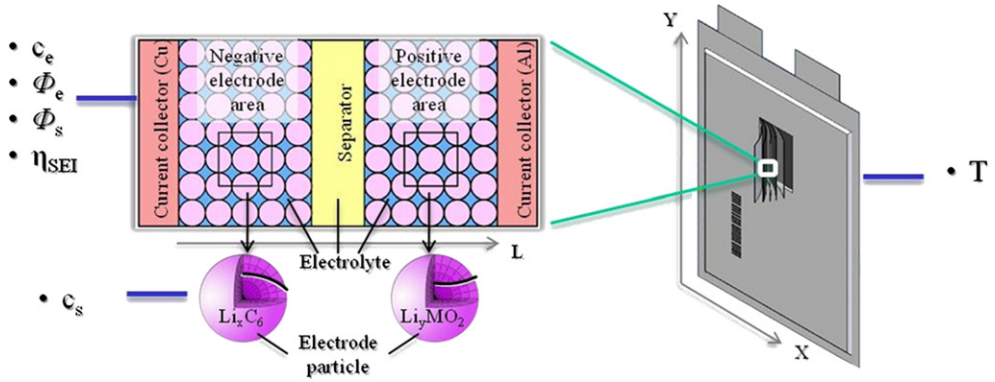

Fig. 2. Simulation setup for a pouch type cell using micro cells.

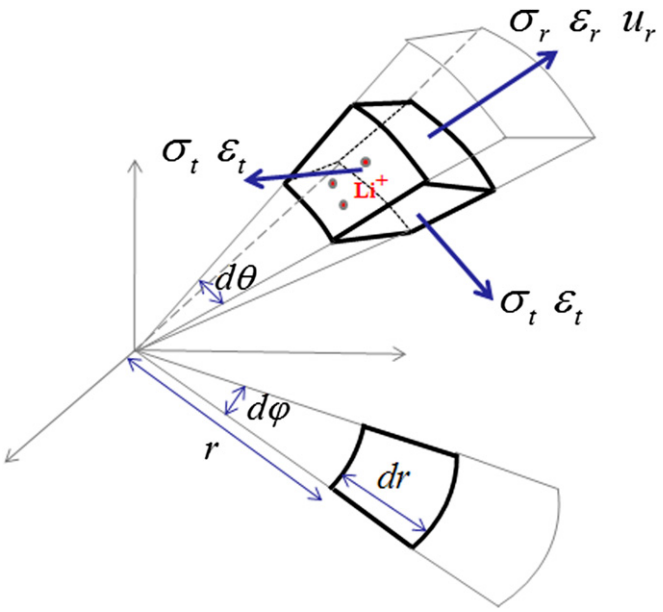

Fig. 3. Localized volume changes and stress generation in a spherical electrode particle.

the ion diffuses in radial direction only and the volume expansion of electrode particles is isotropic.

This work presented here mainly focuses on the analysis of electrochemical and mechanical behaviors coupled in two-way, as highlighted in Fig. 1. The parameters used for the model are listed in Table 1. The input variables are terminal current at the constant current (CC) mode, terminal voltage at the constant voltage (CV) mode and ambient temperature. The outputs are terminal voltage, terminal current, temperature and change of thickness as well as internal variables, such as ion concentrations, stresses, current densities, potentials, etc.

2.1. Ion-induced stress and dimension changes

2.1.1. Stress and displacement in electrode particles

The electrodes are regarded as elastic materials whose expansion is affected by concentration and partial molar volume of ions that inserted. The Hook's law can be applied by adding an extra term that describes the ion-induced changes in normal strains [14];

$$\varepsilon_{ij} = \frac{1}{E}\left[(1+\nu)\sigma_{ij} - \nu\sigma_{kk}\delta_{ij}\right] + \frac{1}{3}c_s\Omega\delta_{ij} \tag{1}$$

where i, j, k take values of 1, 2 or 3. δ_{ij} is the Kronecker delta that is 1 when $i = j$ or 0 when $i \neq j$. c_s is the ion concentration in solid phase. Ω is the Partial Molar Volume (PMV) of Lithium ions in the electrode with a unit of $cm^3\ mol^{-1}$. PMV is considered as the volume change in lithiated electrode when the inserted ion increases by 1 mol. Since the materials of anode and cathode have different lattice constants and structures, the PMV of Lithium ion for anode and cathode has a different value.

The second term in Eq. (1) assumes that the volume expansion induced by ion insertion is isotropic in 3 normal directions. Eq. (1) presents the strain–stress relationship that is similar to the form of equation used for calculation of thermal stress [12,14,18].

The stress equilibrium equation and strain–displacement relationship are

$$\sigma_{ij,i} = 0 \tag{2}$$

$$\varepsilon_{ij} = \frac{1}{2}\left(\frac{\partial u_i}{\partial x_j} + \frac{\partial u_j}{\partial x_i}\right) \tag{3}$$

As each electrode particle is approximated as a one-dimensional symmetric elastic sphere, Eqs. (1)–(3) can be transformed to one-dimensional polar forms as follows;

$$\varepsilon_r = \frac{1}{E}\left[\sigma_r - \nu(\sigma_t + \sigma_t)\right] + \frac{1}{3}c_s\Omega \tag{4}$$

$$\varepsilon_t = \frac{1}{E}\left[\sigma_t - \nu(\sigma_t + \sigma_r)\right] + \frac{1}{3}c_s\Omega \tag{5}$$

where σ_r, σ_t, ε_r and ε_t are stress and strain components in the radial and tangential direction.

The stress equilibrium for a differential volume, as shown in Fig. 3, is

$$\frac{d\sigma_r}{dr} + \frac{2}{r}(\sigma_r - \sigma_t) = 0 \tag{6}$$

The strain–displacement relations are

Table 1
Modeling parameters.

Category	Parameter	Negative electrode	Separator	Positive electrode	Unit
Geometry and volume fractions	Thickness, h_0	50×10^{-4}	25.4×10^{-4}	36.4×10^{-4}	cm
	Particle radius, R_{s0}	1×10^{-4}		1×10^{-4}	cm
	Active material volume fraction, ε_s	0.58		0.5	
	Polymer phase volume fraction, ε_p	0.048	0.5	0.11	
	Conductive filler volume fraction, ε_f	0.04		0.06	
	Porosity, ε_e	0.332	0.5	0.33	
Mechanical properties	Young's modulus, E	15,000		10,000	MPa
	Poisson's ratio, ν	0.3		0.3	
	Fractional expansivity, ω	0.08		0.065	
Li^+ concentrations	Stoichiometry at 0% SOC: $x_{0\%}$, $y_{0\%}$	0.126		0.936	
	Stoichiometry at 100% SOC: $x_{100\%}$, $y_{100\%}$	0.676		0.442	
	Average electrolyte concentration, c_e	1.2×10^{-3}	1.2×10^{-3}	1.2×10^{-3}	mol cm^{-3}
	Exchange current density coefficient, k_{i0}	12.9		6.28	A cm^{-2}
Kinetic and transport properties	Charge-transfer coefficient, α_a, α_c	0.5, 0.5		0.5, 0.5	
	Solid phase diffusion coefficient, D	2.0×10^{-12}		3.7×10^{-12}	$cm^2\ s^{-1}$
	Solid phase conductivity, σ	1		0.1	S cm^{-1}
	Electrolyte phase Li^+ diffusion coefficient, D_e	2.6×10^{-6}	2.6×10^{-6}	2.6×10^{-6}	$cm^2\ s^{-1}$
	Bruggeman's porosity exponent, p	1.5	1.5	1.5	
	Electrolyte phase ionic conductivity, κ	$15.8c_e \exp(-13472c_e^{14})$		$15.8c_e \exp(-13472c_e^{14})$	S cm^{-1}
	Li^+ transference number, t_+^0	0.363	0.363	0.363	

$$\varepsilon_r = \frac{du}{dr} \tag{7}$$

$$\varepsilon_t = \frac{u}{r} \tag{8}$$

where u denotes the displacement in radial direction.

Two boundary conditions are used. Firstly, the radial displacement u at the center of sphere ($r = 0$) is zero since the particle is considered as symmetric sphere. Secondly, the radial stress σ_r at the particle surface ($r = R_{s0}$) is zero since the particle surface is regarded as a free surface. Based on Eqs. (4)–(8) and the boundary conditions, the stress and radial displacement can be solved as a function of r and $c_s(r)$;

$$\sigma_r = \frac{2\Omega E}{3(1-\nu)}\left(\frac{1}{R_{s0}^3}\int_0^{R_{s0}} c_s r^2 dr - \frac{1}{r^3}\int_0^{r} c_s r^2 dr\right) \tag{9}$$

$$\sigma_t = \frac{\Omega E}{3(1-\nu)}\left(\frac{2}{R_{s0}^3}\int_0^{R_{s0}} c_s r^2 dr + \frac{1}{r^3}\int_0^{r} c_s r^2 dr - c_s\right) \tag{10}$$

$$u = \left[\frac{2\Omega(1-2\nu)}{9(1-\nu)}\cdot\frac{3}{R_{s0}^3}\int_0^{R_{s0}} c_s r^2 dr + \frac{\Omega(1+\nu)}{9(1-\nu)}\cdot\frac{3}{r^3}\int_0^{r} c_s r^2 dr\right]\cdot r \tag{11}$$

2.1.2. Effects of SOC on thickness changes of a single cell

The thickness of a cell generally varies at charging or discharging because the volume of an electrode particle is affected by the presence of ions. When a cell is charged, anode particles expand while cathode particles contract. Conversely, cathode particles expand and anode particles contract when a cell is discharged. However, the rates of volume changes in anode and cathode are not the same because the composite anode and composite cathode have different lattice structures, thickness and porosity. As a result, the overall volume of a cell varies as the SOC does.

The change of particle radius, ΔR_s, can be found by setting $r = R_{s0}$ in Eq. (11);

$$\Delta R_s = u(R_{s0}) = \frac{1}{3}\bar{c}_s \Omega R_{s0} \tag{12}$$

where $\bar{c}_s$ is the averaged ion concentration in an electrode particle and R_{s0} is the radius of an electrode particle without expansion caused by lithiation.

The volume changes of composite electrode (anode or cathode) mixed with electrolyte is caused by the volume changes of electrode particles [22], which can be described as follows

$$\frac{V}{V_0} = \left(\frac{V_s}{V_{s0}}\right)^g \tag{13}$$

where V_s and V_{s0} denote the volumes of electrode particles with and without expansion caused by lithiation. V and V_0 denote the volumes of composite electrodes with and without expansion caused by lithiation. g is a swelling coefficient describing how volume changes of particles affect the volumes of composite electrode. However, the value of g is dependent on electrode porosity and the arrangement of particles and is hard to determine. Therefore it is assumed that g is equal to 1 and the volume changes of particles fully contribute to the volume change of composite electrode. Since the volume of spherical particles, V_s, is proportional to R_s^3, Eq. (13) can be linearized using the Taylor series. Perturbation of the volume becomes

$$\Delta V = 3V_0\frac{\Delta R_s}{R_{s0}} \tag{14}$$

For the pouch type of cell used for validation, it is assumed that volume change occurs in the through-the-plane (thickness) direction. Since the area of composite electrodes is A, the volume change in composite electrode is $\Delta V = A\Delta h$. Then, Eq. (14) becomes;

$$\Delta h = 3h_0\frac{\Delta R_s}{R_{s0}} \tag{15}$$

where h_0 denotes the thickness of composite electrode without expansion caused by lithiation, and Δh denotes the thickness increase of composite electrode caused by lithiation. Substitute Eq. (12) to Eq. (15), the change of the thickness is expressed as a function of the average concentration;

$$\Delta h = \Omega h_0 \bar{c}_s \tag{16}$$

On the other hand, the average concentration can be expressed from the stoichiometric numbers and SOC of the cell;

$$\begin{aligned}\bar{c}_{s-} &= (x_{0\%} + (x_{100\%} - x_{0\%}) \times \mathrm{SOC})\cdot c_{s-,\max}\\ \bar{c}_{s+} &= (y_{0\%} + (y_{100\%} - y_{0\%}) \times \mathrm{SOC})\cdot c_{s+,\max}\end{aligned} \tag{17}$$

By substituting Eq. (17) to Eq. (16), we have

$$\begin{aligned}\Delta h_- &= \Omega_- h_{0-} c_{s-,\max}\cdot x_{0\%} + \Omega_+ h_{0-} c_{s-,\max}\cdot(x_{100\%} - x_{0\%})\cdot \mathrm{SOC}\\ \Delta h_+ &= \Omega_+ h_{0+} c_{s+,\max}\cdot y_{0\%} + \Omega_+ h_{0+} c_{s+,\max}\cdot(y_{100\%} - y_{0\%})\cdot \mathrm{SOC}\end{aligned} \tag{18}$$

The effect of SOC on the thickness of electrode can be obtained by taking a derivative on Eq. (18);

$$\begin{aligned}\frac{d\Delta h_-}{d\mathrm{SOC}} &= \Omega_- h_{0-} c_{s-,\max}\cdot(x_{100\%} - x_{0\%})\\ \frac{d\Delta h_+}{d\mathrm{SOC}} &= \Omega_+ h_{0+} c_{s+,\max}\cdot(y_{100\%} - y_{0\%})\end{aligned} \tag{19}$$

Eq. (19) indicates a relationship between the thickness change of a composite electrode (anode or cathode) and the SOC of a cell. The SOC increases at charging and the number of ions in anode increases, so the volume of composite anode increases. Also, $x_{100\%}$ is larger than $x_{0\%}$ and the sign of Eq. (19) for anode is positive. Conversely, cathode loses ions and its volume decreases when SOC increases. Also, $y_{100\%}$ is less than $y_{0\%}$ and the sign of Eq. (19) for cathode is negative.

The maximum ion concentration in anode and cathode can be calculated as

$$\begin{aligned}c_{s-,\max} &= \frac{C_{\mathrm{equi}}}{(x_{100\%} - x_{0\%})\cdot h_{-,\max}\cdot\varepsilon_{s-}\cdot A\cdot F\cdot N} = 0.041\ \mathrm{mol\ cm^{-3}}\\ c_{s+,\max} &= \frac{C_{\mathrm{equi}}}{(y_{0\%} - y_{100\%})\cdot h_{+,\max}\cdot\varepsilon_{s+}\cdot A\cdot F\cdot N} = 0.073\ \mathrm{mol\ cm^{-3}}\end{aligned} \tag{20}$$

where subscripts − and + denote anode and cathode, respectively. C_{equi} is the equivalent capacity and N is the number of micro cells of a single cell. Both values are based on the cell specifications. F is the Faraday constant. The volume fraction of active material of electrode, ε_s, and the stoichiometric numbers at 0% and 100% SOCs are based on Smith and Wang [8]. $h_{-,\max}$ and $h_{+,\max}$ are the maximum

thickness of composite anode or cathode caused by the expansion caused by lithiation.

When the electrode is fully lithiated, the volume of electrode particle expands by a factor of $(1+\omega)$, where ω is the fractional expansivity of the electrode material according to Christensen and Newman [10,11], as shown in Eq. (21);

$$\frac{V_{s,max}}{V_{s0}} = \left(\frac{R_{s,max}}{R_{s0}}\right)^3 = 1+\omega \tag{21}$$

Then, the maximum thickness of composite electrode results in

$$h_{max} = (1+\omega)h_0 \tag{22}$$

where h_0 is obtained from the cell specification. Since no other components (separator or current collector) in the battery are affected by SOC, the thickness change of a single cell can be derived from the thickness changes of all composite electrodes in anode and cathode;

$$\Delta h_{cell} = N(\Delta h_- + \Delta h_+) \tag{23}$$

Eq. (23) assumed that there is no compression force from the pouch packaging material when the cell expands. Since the packaging material is a resilient plastic, the maximum pressure exerted by the packaging material to the cell is smaller than the atmosphere pressure, based on an order of magnitude analysis provided in the Appendix. Therefore, the separator should have no deformation and the response of inner and outer micro cells should experience the same mechanical response.

By combining Eqs. (18)–(20) and (23), the thickness change of a cell due to SOC can be derived as follows

$$\frac{d\Delta h_{cell}}{dSOC} = \frac{C_{equi}}{AF}\left(\frac{\Omega_-}{\varepsilon_{s-}(1+\omega_-)} - \frac{\Omega_+}{\varepsilon_{s+}(1+\omega_+)}\right) \tag{24}$$

The unknown PMVs of ions in anode and cathode, Ω_- and Ω_+, can be derived from the known fractional expansivity ω [10,11]. Firstly obtain the maximum deviation of particle radius from Eq. (12);

$$\Delta R_{s,max} = \frac{1}{3}\bar{c}_{s,max}\Omega R_{s0} \tag{25}$$

Secondly substitute Eq. (25) to Eq. (21). The PMVs are now derived for both anode and cathode;

$$\begin{aligned}\Omega_- &= \frac{3}{c_{s-,max}}\left[(1+\omega_-)^{\frac{1}{3}}-1\right] = 2.77\ \mathrm{cm^3\ mol^{-1}}\\ \Omega_+ &= \frac{3}{c_{s+,max}}\left[(1+\omega_+)^{\frac{1}{3}}-1\right] = 0.93\ \mathrm{cm^3\ mol^{-1}}\end{aligned} \tag{26}$$

where $c_{s-,max}$ and $c_{s+,max}$ are calculated from Eq. (20), and the values of ω_- and ω_+ are 0.08 and 0.06, respectively [10,11].

2.2. Ion transport and charge conservations

2.2.1. Ion transport in electrode considering stress-induced diffusion

Based on the principle of thermal dynamics, chemical potential of a substance is affected by the pressure that is equivalent to hydrostatic stress, σ_h, for solid materials [21]. According to this theory, Yang [13] and Zhang et al. [14] derived the species flux of ion in electrode particles driven by concentration and stress gradient;

$$J = -D\left(\nabla c_s - \frac{\Omega c_s}{RT}\nabla\sigma_h\right) \tag{27}$$

where the hydrostatic stress, σ_h, can be expressed as

$$\sigma_h = \frac{1}{3}(\sigma_r + \sigma_t + \sigma_t) \tag{28}$$

The change of ion concentration in a differential volume is equal to the gradient of species flux;

$$\frac{\partial c_s}{\partial t} + \nabla\cdot J = 0 \tag{29}$$

Substitute Eq. (29) with Eq. (27) and Eq. (28) and then take derivatives in spherical coordinates, the equation of the material balance in electrode particles results in [14];

$$\begin{aligned}\frac{\partial c_s}{\partial t} = D\left(\frac{\partial^2 c_s}{\partial r^2} + \frac{2}{r}\frac{\partial c_s}{\partial r}\right) - \frac{2D\Omega E}{9RT(1-\nu)}\\ \times\left[\left(\frac{\partial c_s}{\partial r}\right)^2 + c_s\left(\frac{\partial^2 c_s}{\partial r^2} + \frac{2}{r}\frac{\partial c_s}{\partial r}\right)\right]\end{aligned} \tag{30}$$

where the first and second term denotes the diffusion caused by the concentration gradient and the stress gradient respectively.

2.2.2. Ion transport in electrolyte

The balance of materials in electrolyte is affected by the gradient of ion concentrations. When the electrodes have pores that are filled with electrolyte, the balance should consider the porosity of the material. Accordingly, the diffusion coefficient is redefined considering the porosity as follows;

$$D_e^{eff} = D_e\cdot\varepsilon_e \tag{31}$$

where the diffusion coefficient, D_e, is a constant. The material balance for the electrolyte considering the porosity [23] is

$$\frac{\partial(\varepsilon_e c_e)}{\partial t} = \frac{\partial}{\partial x}\left(D_e^{eff}\cdot\frac{\partial}{\partial x}c_e\right) + \frac{1-t_+^0}{F}j^{Li} = 0 \tag{32}$$

where c_e is the concentration of lithium ion in electrolyte, F is the Faraday's constant, t_+^0 is the initial transference number, ε_e is the porosity, and j^{Li} is the current density.

2.2.3. Charge conservation in electrode and electrolyte

The amount of charges produced in oxidation process should be equal to those consumed in reduction process. This relationship is described using the Ohm's law and expressed as a function of currents and potential gradients [23]. Ions transport in electrolyte is governed by the Nernst–Planck equation as shown in the following equation;

$$\frac{\partial}{\partial x}\left(\kappa_e^{eff}\cdot\frac{\partial}{\partial x}\varphi_e\right) + \frac{\partial}{\partial x}\left(\kappa_D^{eff}\cdot\frac{\partial}{\partial x}(\ln c_e)\right) + j^{Li} = 0 \tag{33}$$

where φ_e is the electrolyte potential, κ_D^{eff} is the effective electrolyte conductivity and κ_D^{eff} is the concentration driven diffusion conductivity.

The charge transport in solid electrode has no diffusion terms, which is solely governed by the Ohm's law

$$\frac{\partial}{\partial x}\left(\sigma^{eff}\cdot\frac{\partial}{\partial x}\varphi_s\right) = j^{Li} \tag{34}$$

where σ^{eff} is the solid phase electronic conductivity.

2.3. Energy conservation

Cell temperature affects the cell performance and the degradation of materials, which is described using the energy equation;

$$C_p m \frac{\partial T}{\partial t} = Q_{rev} + Q_{irr} + Q_{convec} \quad (35)$$

where C_p and m are the heat capacity and mass. Q_{rev}, Q_{irr} and Q_{convec} are the reversible heat source, the irreversible heat source, and the heat convection rate, respectively.

The reversible heat is a result of change of entropy during a chemical reaction ($T\Delta S$). Song and Evans [7] expressed the rate of the heat generated as

$$Q_{rev} = \int_V j^{Li} \cdot T \cdot \frac{\partial U_{OCV}}{\partial T} dV \quad (36)$$

Since the irreversible heat generation, Q_{irr}, includes a Joule heating and a heat of mixing, Xiao and Choe [23] proposed the following modification. The electrochemical energy can be expressed as follows;

$$E_{chem} = -\varepsilon_{s+} \cdot F \cdot \int_V c_{s+} \cdot U_{equi,+} \cdot dV - \varepsilon_{s-} \cdot F \cdot \int_V c_{s-} \cdot U_{equi,-} \cdot dV \quad (37)$$

The power contributing to the increase of chemical energy can be obtained by differentiating the electrochemical energy with respect to time;

$$p_{chem} = \frac{dE_{chem}}{dt} \quad (38)$$

The irreversible heat generation rate for a micro cell is the difference between the electrical power supplied to the cell ($-V_T \cdot I$) and the power contributing to the increase of chemical energy (P_{chem})

$$Q_{irr} = -V_T \cdot I - P_{chem} \quad (39)$$

When charging, $0 < P_{chem} < -V_T \cdot I$. When discharging, $P_{chem} < -V_T \cdot I < 0$. Therefore, Q_{irr} is always positive. Q_{irr} calculated from Eq. (37)–(39) includes the Joule heating generated in electrode, electrolyte and their interfaces. Q_{irr} also includes the heat of mixing caused by concentration relaxation in electrode. However, the heat generation caused by concentration relaxation in electrolyte is neglected in this work since the amount of Li ion in electrolyte is much less than that in electrode.

In addition, a heat transfer by convection is considered

$$Q_{convec.} = h_c \cdot (T - T_\infty) \quad (40)$$

where h_c ,T and T_∞ denote the convective heat transfer coefficient, cell temperature and ambient temperature, respectively.

2.4. Equilibrium potentials and Butler–Volmer equation

The equilibrium potential of an electrode is a function of stoichiometric number which is determined by the ratio of ion concentration in solid phase to its maximum value. Smith and Wang [8] approximated the negative equilibrium potential using the equation as a function of stoichiometric number;

$$\begin{aligned} U_{equi,-}(x) = {} & 8.00229 + 5.0647\,x - 12.578\,x^{1/2} \\ & -8.6322\,e-4x^{-1} + 2.1765\,e-5x^{3/2} \\ & -0.46016\,\exp(15(0.06-x)) \\ & -0.55364\,\exp(-2.4326 \\ & \times(x-0.92)) \end{aligned} \quad (41)$$

The positive equilibrium potential is obtained by adding negative equilibrium potential with open circuit voltage (OCV) obtained by experiment

$$U_{equi,+}(y) = U_{OCV} + U_{equi,-}(x) \quad (42)$$

The current produced by chemical reactions is a function of overpotential governed by the Butler–Volmer equation, which simplified by a linear equation given in Eq. (43);

$$j^{Li} = a_s i_0 \frac{(\alpha_- + \alpha_+)F}{RT}\eta \quad (43)$$

This linear relationship between j^{Li} and η in Eq. (43) is applicable only if the activation overpotential is relatively low (e.g., $\eta < 10$ mV). For the cell studied in this work, η is around several milli-volts at 7C rate. This linear equation eases the charge conservation equation to converge and reduces the computational time. The activation overpotential η in Eq. (43) is the difference between the potential between electrode and electrolyte and the equilibrium potential;

$$\eta = \phi_s - \phi_e - U_{equi} \quad (44)$$

2.5. Initial and boundary conditions

Since the ion concentration inside the particles is spherically symmetric and does not have any sources, the gradient of ion concentration at the center is zero. The outer boundary of electrode particles is determined by the rate of the reaction

$$\begin{aligned} r^2 \frac{\partial c_s}{\partial r}\Big|_{r=0} &= 0 \\ -D_s \frac{\partial c_s}{\partial r}\Big|_{r=R_{s0}} &= \frac{j^{Li}}{a_s F} \end{aligned} \quad (45)$$

Again, the radial displacement at the center of particle is zero and the radial stress at the surface of particle is zero

$$\begin{aligned} u|_{r=R_{s0}} &= 0 \\ \sigma_r|_{r=0} &= 0 \end{aligned} \quad (46)$$

Since there is no electrolyte flow at the left and right boundaries of a micro cell, the change in electrolyte concentration is equal to zero

$$\frac{\partial c_e}{\partial x}\Big|_{x=0} = \frac{\partial c_e}{\partial x}\Big|_{x=L} = 0 \quad (47)$$

The boundary conditions for the potentials of electrode is

$$-\sigma_-^{eff}\frac{\partial \varphi_s}{\partial x}\Big|_{x=0} = -\sigma_+^{eff}\frac{\partial \varphi_s}{\partial x}\Big|_{x=L} = \frac{I}{A} \quad \frac{\partial \varphi_s}{\partial x}\Big|_{x=h_-} = \frac{\partial \varphi_s}{\partial x}\Big|_{x=h_+} = 0 \quad (48)$$

where the σ^{eff} is the conductivity and φ_s is the solid phase potential. $x = 0$ represents the interface between the electrode and negative current collector, and $x = L$ represents the interface between the electrode and positive current collector. $x = h_-$ and $x = h_+$ represent the interface between separator and electrode at the negative and positive sides respectively. In addition, the boundary conditions for the potentials of electrolyte is

$$\frac{\partial \varphi_e}{\partial x}\Big|_{x=0} = \frac{\partial \varphi_e}{\partial x}\Big|_{x=L} = 0 \quad (49)$$

The initial conditions of various variables are determined from the initial lithium ion concentration in the electrodes. The initial ion concentration is assumed with no gradient and expressed as a function of SOC, as shown in Eq. (17).

2.6. Numerical method

The equations are discretized and coded using MATLAB. The anode, separator and cathode are meshed with 25 grids in the

direction of thickness, and each electrode particle is meshed with 10 grids in the radial direction. The conservation of charge in electrolyte (Eqs. (33) and (34)) across the cell are firstly solved. The resulting phase and equilibrium potentials are used to calculate overpotential across the cell and then the reaction rate j^{Li} by means of the Butler–Volmer equation (Eq. (43)). The solved potentials, φ_s and φ_e, as well as reaction rate, j^{Li}, provide the inputs for the calculating conservation of mass in electrode (Eq. (30)) and electrolyte (Eq. (32)), which is used to determine the change in concentration with each time step. After the ion concentrations are solved, the stress and displacement in electrode particles as well as the change of cell thickness are solved at last using Eqs. (9)–(11) and Eq. (24) since they are functions of ion concentrations in solid phase.

3. Experimental setup

A test station was designed, constructed and calibrated. The schematic diagram of the test station is shown in Fig. 4, where a programmable power supply and a programmable electronic load were used to generate a charging and discharging profile controlled by Labview. At the same time, the terminal current and voltage, temperature, and thickness of the cell were measured and processed. Tests were conducted in a thermal chamber where the ambient temperature was set to 25 °C.

Since it is difficult to measure stress generation in electrodes for commercial cells, change of thickness of the cell was measured by two LVDTs. The two LVDTs were placed on both sides of battery with a possibility to measure the thickness at different locations of the cell and robustly supported by a fixture, as shown in Fig. 5. It should be noted that no gas evolutions were observed during the tests. In addition, the pressure produced by possible gas evolution does not cause any measurement error since the spring of LVDTs can impose a pressure around several hundreds of Kilo-Pascal on the cell. In this paper, only the thickness at the center of battery is measured and used to compare with results of simulations. The device is in synchronization with the test station, so the change of cell thickness under cycling can be recorded during testing.

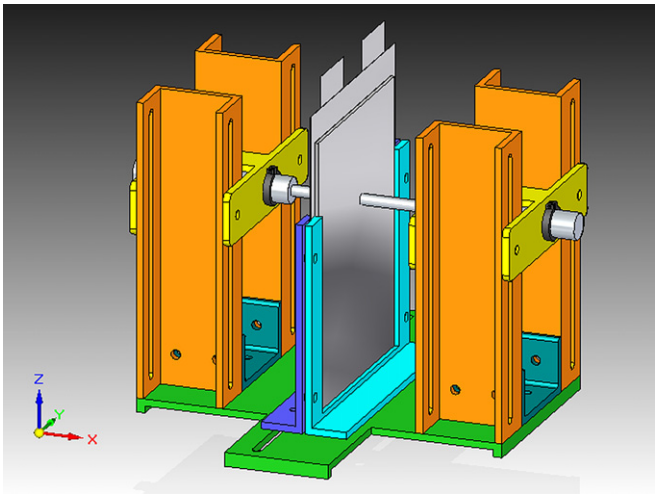

Fig. 5. Designed fixture for the measurements of thickness using 2 LVDTs.

4. Validation and analysis

4.1. Experimental validation of volume expansion

The first experimental data collected using the device and the simulated data at a constant temperature are shown in Fig. 6, where the thickness is a function of SOC. The thickness tends to follow the SOC, as expected. When SOC increases, the cathode loses ions while the anode gains ions, so the anode particles expand and cathode particles contract. In fact, the volume change rate of anode is larger than that of cathode, so the overall thickness of the cell increases with increasing SOC.

The experimental data shows that the change of thickness is not linear to the change of the SOC. The data can be divided into three different regions as the SOC increases. The thickness of cell increases rapidly in the low range of SOC (0–0.4), which agrees with the finding from Ohzuku et al. [24] and Hardwick et al. [25]. Then it becomes flat for the mid-range of SOC (0.4–0.7) and finally increases again when SOC is larger than 0.7.

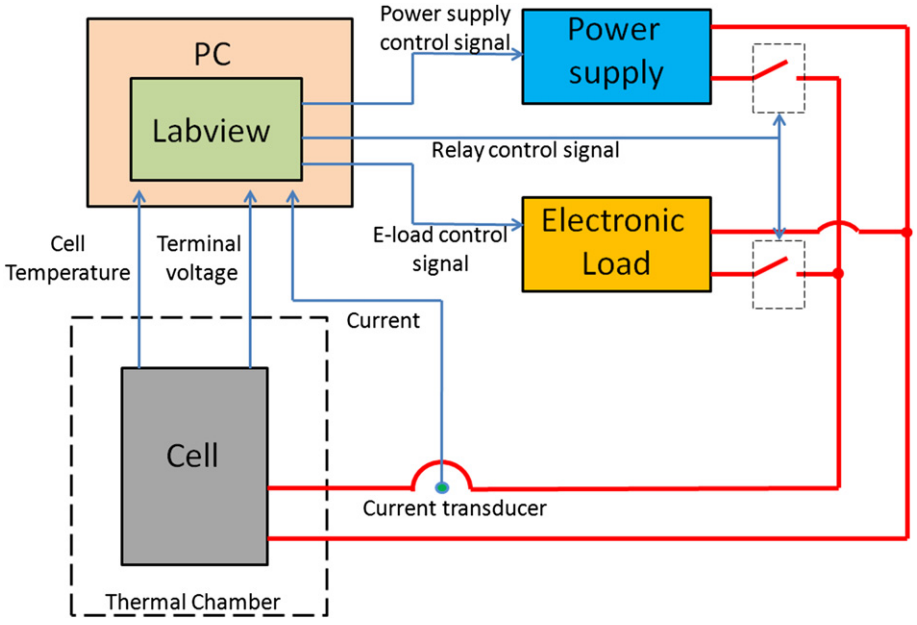

Fig. 4. Schematic diagram of a test station.

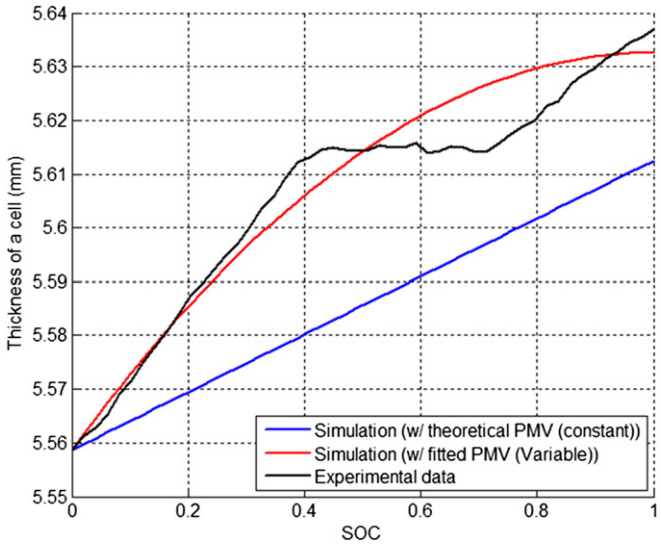

Fig. 6. Comparison between simulated and experimental thickness versus SOC.

The blue curve plotted in Fig. 6 shows a simulated thickness of the cell using the theoretical PMVs based on Eqs. (24) and (26). Since it is assumed that the PMVs in anode and cathode are constant and the change of porosity is negligible, the thickness increases linearly with the SOC. Mismatch of the experiments and simulations may be caused by the inaccurate values of fractional expansivity, ω, and the assumption that the expansion of lattice structure of electrodes is linear.

Since the graphite experiences the most expansion in low SOC region [24,25], which agrees with our experimental data, the PMV of ion in anode could be regarded as being negatively proportional to SOC, while the PMV in the cathode side is preserved as constant. The red curve with this fitting is shown in Fig. 6, where the theoretical PMV is modified as follows and used to calculate the final thickness;

$$\Omega_{-,\text{fitted}} = 2.24\cdot\Omega_{-} - 2.3\cdot\text{SOC} \tag{50}$$

where Ω_{-} is the original PMV obtained from the Eq. (26).

4.2. Experimental validation of the model at low C rates

Fig. 7 shows the simulated current, terminal voltage, temperature, thickness and maximum anode stress under cycling, which are compared with the experimental data. The current rates applied are 0.5C, 1C and 2C for each cycle respectively. Each cycle includes a constant current discharge, a constant current charge and a constant voltage charge along with a 10 min resting period between charging and discharging.

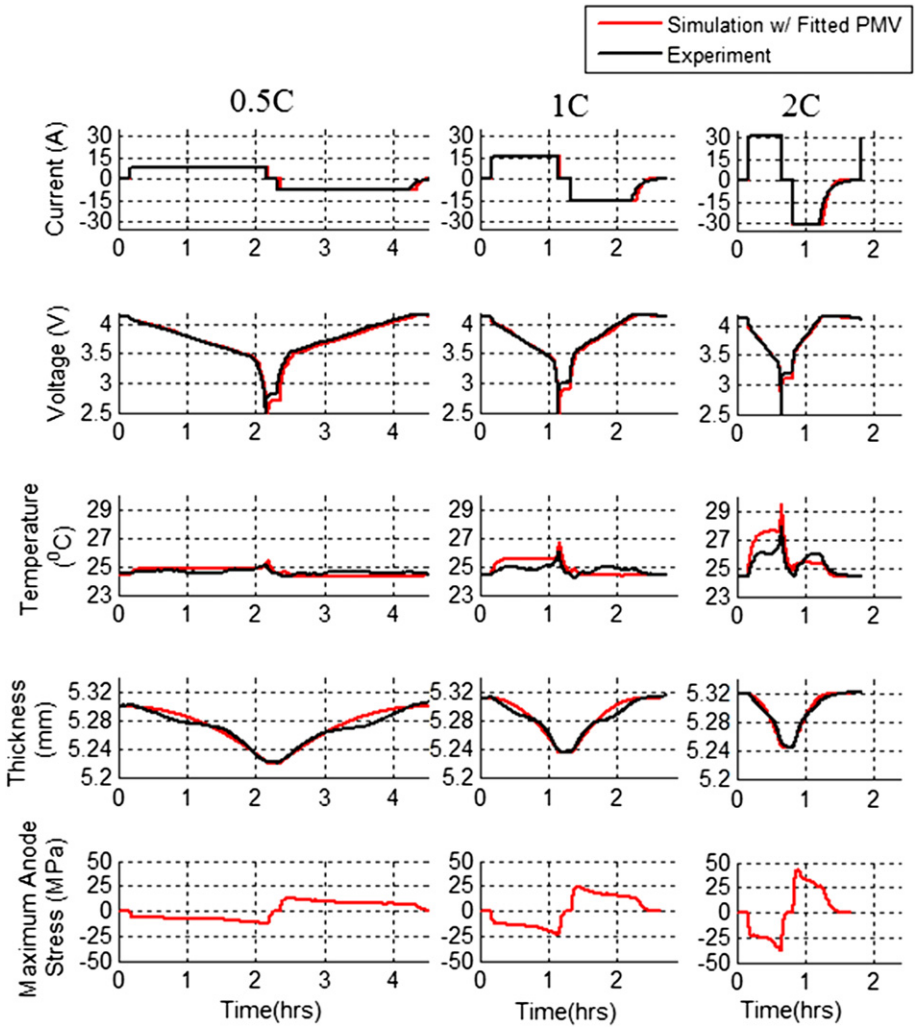

Fig. 7. Experimental validations at 0.5C, 1C and 2C cycles.

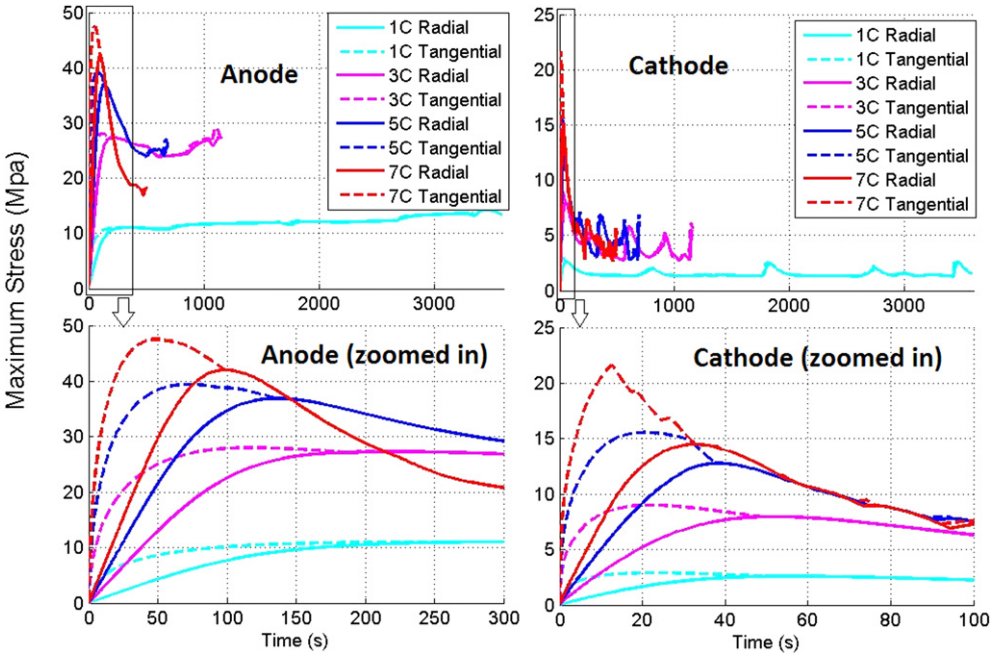

Fig. 8. Maximum stress (absolute values) as a function of time.

Comparison shows that the current and voltage are relatively in good match. However, some discrepancies in temperature responses are observed, which might be caused by the inaccurate values of convective heat transfer coefficient. The temperature rises are higher during discharge than charge because the entropy heating is exothermic during discharge and endothermic during charge. In addition, the thickness is only affected by the SOC, but not current rate. Current at high C rate leads to a high amplitude of stress because the stress follows the increase of the gradient of ion concentration in electrode particles. During resting periods, the gradient of ion concentration gets low, so the stress decreases and tends to vanish.

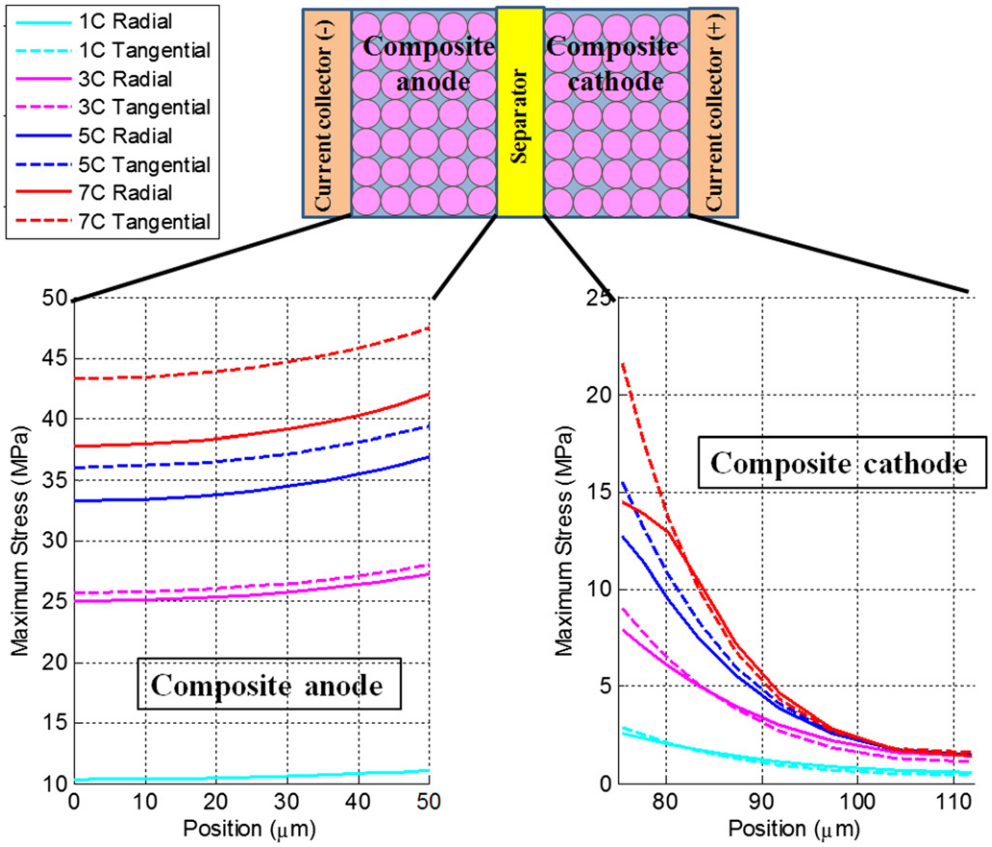

Fig. 9. Maximum stress (absolute values) as a function of the thickness of a micro cell.

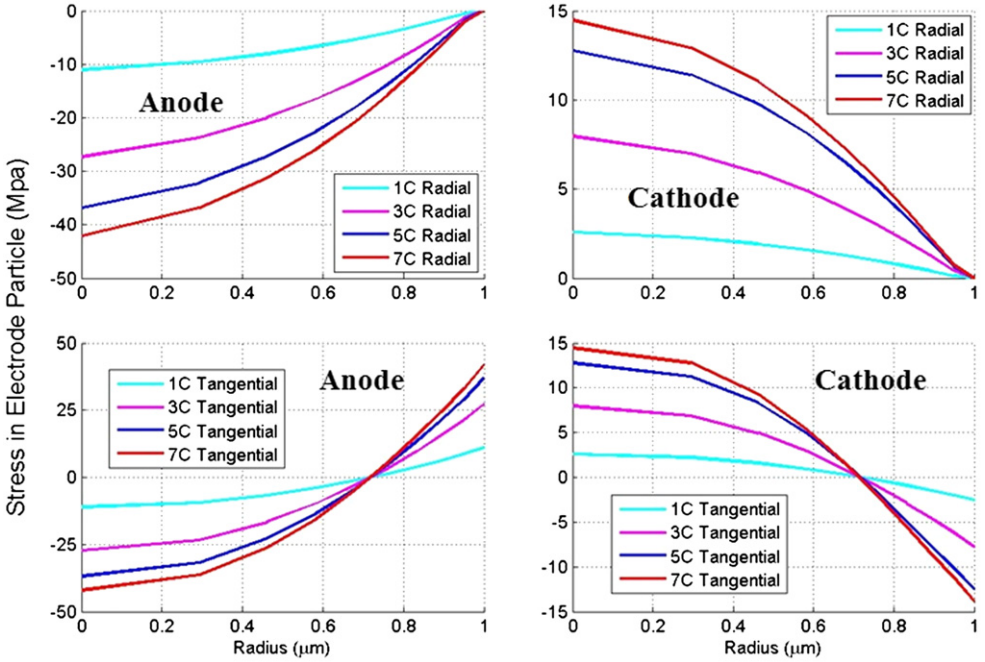

Fig. 10. Stress as a function of particle radius.

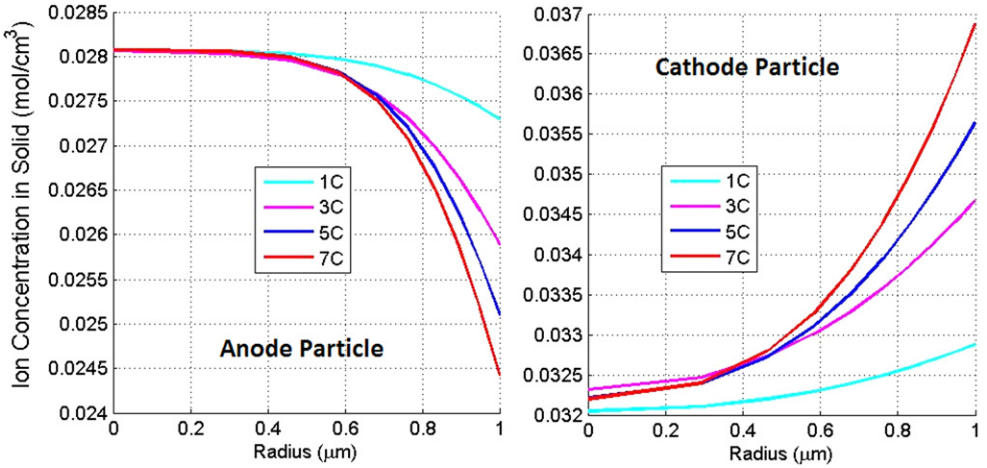

Fig. 11. Ion concentration in solid particles (same particles selected in Fig. 10).

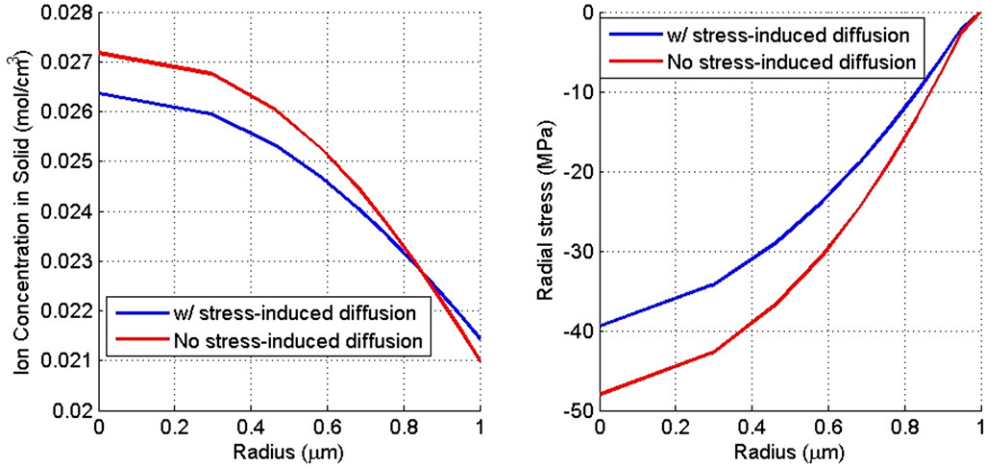

Fig. 12. Effect of stress-induced diffusion on ion concentration and radial stress during 7C discharge.

4.3. Analysis of stress generation at high C rates

In this part, stress generations at high current rates are analyzed with respect to its time evolution, distribution in composite electrodes and electrode particles, as well as its effect on the cell performance. As indicated in Fig. 7, the direction of current at charging or discharging only affects the direction of stress, so only discharge process is considered to analyze the stress generation.

Time evolution of the maximum stress in anode or cathode under different discharge current is shown in Fig. 8. When the current rate is low, for example, 1C, the maximum stress increases at the beginning of discharge and tends to stay constant afterward. When current rate is high, for example, 3C, 5C and 7C, the maximum stress increases significantly to an extreme value and then slowly goes down.

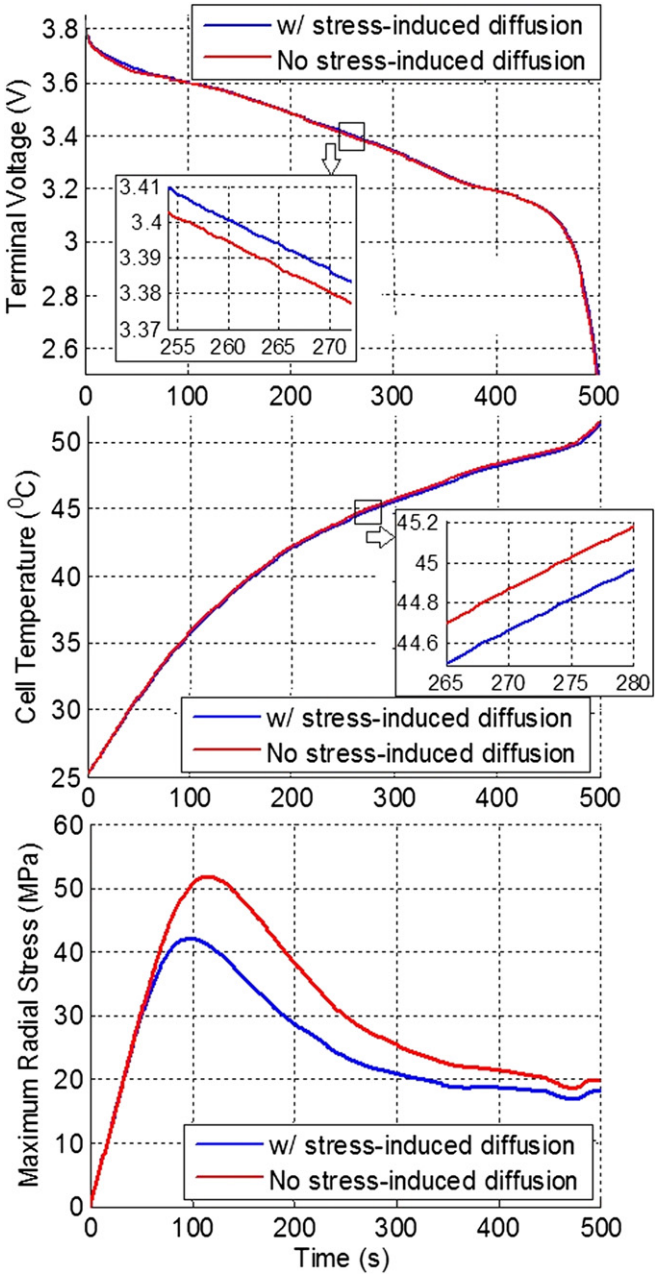

Fig. 13. Effect of stress-induced diffusion on terminal voltage, cell temperature and maximum radial stress under 7C discharge.

The maximum stress in tangential direction, σ_t, is slightly larger than the stress in radial direction, σ_r. The stress generated in anode is almost twice larger than that in cathode, since anode material has a larger Young's modulus and a higher PMV of Li ion. The simulation indicates that a high current rate is most likely to cause electrode material failures at the beginning of discharge and charge.

Maximum stress as a function of the thickness of micro cell is shown in Fig. 9. The domain from 0 to 50 μm indicates the composite anode mixed with electrolyte, the domain from 50 μm to 75 μm indicates a separator where stress is not considered, and the domain from 75 μm to 112 μm indicates the composite cathode mixed with electrolyte. The plotted stress at each position is the maximum value of the stress in the local electrode particles. Each stress curve is obtained at the time instant when extreme value is reached in Fig. 8.

The results show that the tangential stress is slightly higher than the radial stress and the stress in anode is larger than that in cathode, as shown in Fig. 9. In addition, the magnitude of stress is dependent on the locations of composite electrode. The highest value of stress is on the electrode particles in contact with the separator, which implies that the material failure by crack or fracture is more likely to happen in the electrode particles that are close to the separator. This fact is in line with the experimental work done by Kostecki and McLarnon [26], who showed that the graphite particles near the separator become more disordered under cycling. Horn and White [27] also found cracks in electrode particles near the separator by SEM images at the cross-section of a cell.

In order to study stress distributions in particles, particles near the separator are selected and the stress distributions in a single electrode particle are shown in Fig. 10. Each stress curve is obtained at the instant when extreme value is reached in Fig. 8. At discharging, the anode electrode loses ions so that the particle has a negative radial stress and compressed in radial direction. The magnitude of the radial stress becomes highest at the center of sphere and decays to zero at the surface. In the tangential direction of anode particle, the stress is compressive in the inner part of sphere and tensile in the outer part of sphere. The maximum magnitude of tangential stress is similar to radial stress. Conversely, in the cathode particles, the directions of stresses are opposite to those in the anode since the cathode gains ions. The magnitude of stress in cathode is smaller than anode due to different Young's modulus and PMVs of ion.

The stresses are generated by the inhomogeneous distribution of ion concentration in electrode particles. As described in Eqs. (9) and (10), the distribution of ion concentration determines the magnitude and direction of stress. In most cases, high gradient of ion concentration would induce large stress. Radial stress is proportional to the difference between averaged ion concentration in the entire particle and averaged ion concentration in the "localized region", as indicated in Eq. (9).

The ion concentrations in the electrode particles selected in Fig. 10 are plotted in Fig. 11. It is observed that a high current induces a large gradient of ion concentration in electrodes, and in turn results in a large stress.

4.4. Analysis of the effects of stress-induced diffusion on the cell performance

The effects of electrochemical behavior on stress generation have been analyzed in the previous sessions. According to the Eq. (27), the gradient of hydrostatic stress influences diffusion flux of ions in electrode. Therefore, the species conservation equation gains an extra term to consider the stress-induced diffusion, as shown in Eq. (30). Based on the equation, the effects of stress-induced diffusion on the cell performance have been studied.

The ion concentrations and radial stresses in an anode particle with and without considering stress-induced diffusion are shown

in Fig. 12. When stress-induced diffusion is considered, the gradient of ion concentration and the magnitude of radial stress become smaller. The result shows that stress could help to improve ion diffusion in electrode particles to some extent.

The terminal voltage, cell temperature and maximum radial stress with and without considering stress-induced diffusion are shown in Fig. 13. The effect of stress-induced diffusion on the terminal voltage and cell temperature is negligible. However, the maximum radial stress is obviously reduced by stress-induced diffusion, since the stress enhances diffusion flux and decreases the gradient of ion concentration in electrode, which is in coincidence with results from Christensen [20]. It is reported that stress-induced diffusion has little effect on terminal voltage, but is important to analyze stress generations.

5. Conclusions

A new dynamic model for a pouch type of LiPB is developed using electrochemical, thermal and mechanical principles. The model is used to analyze terminal and thermal behaviors as well as dimensional changes under different cell operation conditions. Testing equipment is designed to measure the thickness changes, terminal voltage, current and cell temperature that are used to validate the model.

Key findings are as follows:

- The battery thickness is a function of SOC at a constant temperature. When SOC changes from 0 to 100%, the thickness of the battery increases by 1.2%. This is mainly because of the anode material that has a larger expansion rate when ions are intercalated compared to that of the cathode material.
- Stress tends to follow the increase of the ion concentration gradient in an electrode. As a result, high C rate leads to high amplitude of stress. During resting periods, the gradient of the ion concentration gets low, so the stress decreases and vanishes.
- Stress in anode is higher than that in cathode particles because of different material properties.
- At a high C rate, stress might reach its maximum value at the beginning of charge and discharge.
- The highest stress is generated particularly in the electrode particles near the separator, where cracking and fracture are most likely to take place.
- The stress-induced diffusion could enhance the ion diffusion in an electrode and reduces the gradient of ion concentration. However, it has little effects on the macro-scale quantities, such as terminal voltage and cell temperature.

Future work will include effects of temperature on the volume expansion that might be dominant in high C rate operations.

Acknowledgment

This project is funded by General Motor Corporation. The authors do appreciate the financial support and technical discussions.

Appendix

In order to estimate the effect of compression force from the pouch packaging material on the cell expansion, an order-of-magnitude analysis is provided as below. A schematic diagram of the cell geometry with packaging material is depicted in Fig. 14. At charging, the cell expands and the packaging material expands as well. This process is depicted in Fig. 15. At 0% SOC, the cell has the smallest thickness. The circumference of the packaging material results in

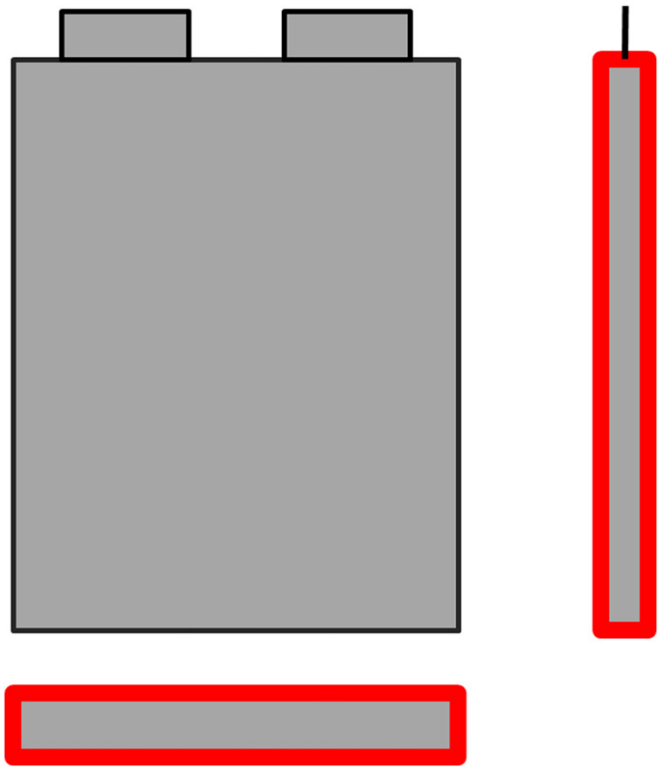

Fig. 14. Front view, side view and bottom view of the cell with packaging material marked by red (The dimensions are not to scale). (For interpretation of the references to color in this figure legend, the reader is referred to the web version of this article.)

$$l_{\text{pack},0} = 2w + 2h_{\text{cell},0} = 2 \times 20 \text{ cm} + 2 \times 0.5322 \text{ cm} = 41.064 \text{ cm} \quad (51)$$

At 100% SOC, the thickness of cell increases to a maximum value and the packaging material should have the largest deformation. The circumference of packaging material is changed to

$$l_{\text{pack,max}} = 2w + 2h_{\text{cell,max}} = 2 \times 20\,\text{cm} + 2 \times 0.5376\,\text{cm} = 41.075\,\text{cm} \quad (52)$$

When the SOC changes from 0% to 100%, the strain of the packaging material can be calculated based on the changes of the circumferences;

$$\varepsilon_{\text{pack}} = \frac{l_{\text{pack,max}} - l_{\text{pack},0}}{l_{\text{pack},0}} = 2.63 \times 10^{-4} \quad (53)$$

The stress of packaging material can be calculated using the Hook's law where the Young's modulus is needed. The Young's modulus of the packaging material is several GPa because the packaging material is made from plastics. For example, the stress generated in the packaging can be calculated under the assumption that its Young's modulus is 5000 MPa;

$$\sigma_{\text{pack}} = E_{\text{pack}}\varepsilon_{\text{pack}} = 5000 \text{ MPa} \times 2.63 \times 10^{-4} = 1.32 \text{ MPa} \quad (54)$$

Free body diagrams for the packaging material and cell are depicted in Fig. 16. The force is only analyzed in x_2 direction at an equilibrium state. The tension on the packaging material is the same as the compression on the cell;

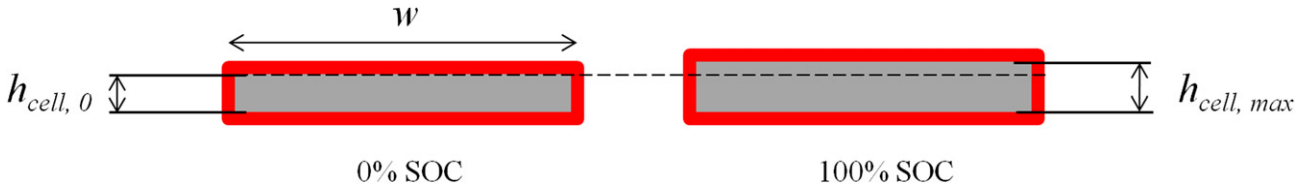

Fig. 15. Bottom view of schematic diagram of cell expansion (The dimensions are not to scale).

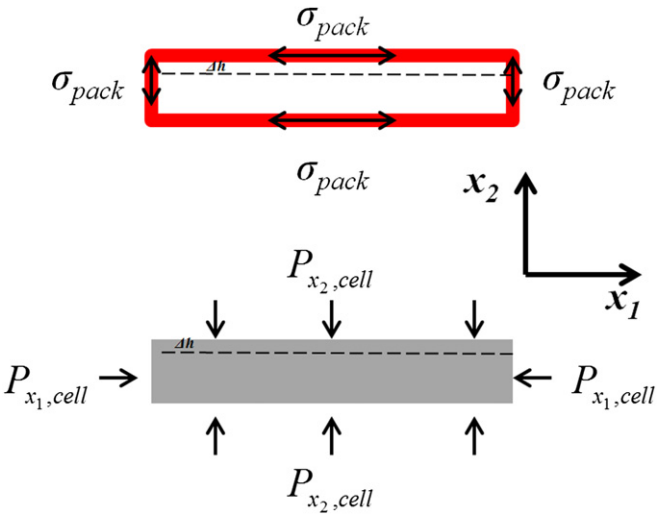

Fig. 16. Free body diagrams of the packaging material and cell (bottom view).

$$F_{x_2,\mathrm{pack}} = F_{x_2,\mathrm{cell}} \tag{55}$$

The tension on the packaging can be calculated by multiplying σ_{pack} by its area, A_{pack}. Since there are two edges, then

$$F_{x_2,\mathrm{pack}} = 2\sigma_{\mathrm{pack}}A_{\mathrm{pack}} = 2\sigma_{\mathrm{pack}}h_{\mathrm{pack}}w = 84.5\mathrm{N} \tag{56}$$

where h_{pack} is the thickness of packaging and equal to 0.16 mm. The compression on the cell is calculated by a multiplication of the pressure exerted on the cell by the area of cell

$$F_{x_2,\mathrm{cell}} = P_{x_2,\mathrm{cell}}A_{\mathrm{cell}} = P_{x_2,\mathrm{cell}} \times 0.03\ \mathrm{m}^2 \tag{57}$$

Therefore, the pressure exerted on the cell in the thickness direction (x_2 direction) can be derived from Eq. (55)–(57);

$$P_{x_2,\mathrm{cell}} = 2.8 \times 10^{-3}\ \mathrm{MPa} \tag{58}$$

Since the pressure exerted on the cell from the packaging material is much smaller than the atmosphere pressure (0.1 MPa), the volume expansion of the cell is not affected by this pressure. Therefore, it is valid to neglect the compression from the pouch packaging material on the cell expansion, as shown in Eq. (23).

References

[1] M. Doyle, T. Fuller, J. Newman, J. Electrochem. Soc. 140 (1993) 1526–1533.
[2] T. Fuller, M. Doyle, J. Newman, J. Electrochem. Soc. 141 (1994) 1–10.
[3] M. Doyle, T. Fuller, J. Newman, Electrochim. Acta 39 (1994) 2073–2081.
[4] S. Stewart, J. Newman, J. Electrochem. Soc. 155 (2008) A458–A463.
[5] S. Steward, J. Newman, J. Electrochem. Soc. 155 (2008) F13–F16.
[6] G. Nagarajan, J. Zee, J. Electrochem. Soc. 145 (1998) 771–779.
[7] L. Song, J. Evans, J. Electrochem. Soc. 147 (2000) 2086–2095.
[8] K. Smith, C. Wang, J. Power Sources 160 (2006) 662–673.
[9] Y. Chen, J. Evans, J. Electrochem. Soc. 140 (1993) 1833–1838.
[10] J. Christensen, J. Newman, J. Solid State Electrochem. 10 (2006) 293–319.
[11] J. Christensen, J. Newman, J. Electrochem. Soc. 153 (2006) A1019–A1030.
[12] S. Prussin, J. Appl. Phys. 32 (1961) 1876–1881.
[13] F. Yang, Mater. Sci. Eng. A 409 (2005) 153–159.
[14] X. Zhang, W. Shyy, A. Sastry, J. Electrochem. Soc. 154 (2007) A910–A916.
[15] X. Zhang, A. Sastry, W. Shyy, J. Electrochem. Soc. 155 (2008) A542–A552.
[16] S.J. Harris, R.D. Deshpande, Y. Qi, I. Dutta, Y. Cheng, J. Mater. Res. 25 (2010) 1433–1440.
[17] R.E. Garcia, Y. Chiang, W.C. Carter, P. Limthongkul, C.M. Bishop, J. Electrochem. Soc. 152 (2005) A255–A263.
[18] S. Golmon, K. Maute, M.L. Dunn, Comput. Struct. 87 (2009) 1567–1579.
[19] A.F. Bower, P.R. Guduru, V.A. Sethuraman, J. Mech. Phys. Solids 59 (2011) 804–828.
[20] J. Christensen, J. Electrochem. Soc. 157 (2010) A366–A380.
[21] J.C.M. Li, Metall. Trans. A 9A (1978) 1353–1380.
[22] P.M. Gomadam, J.W. Weidner, J. Electrochem. Soc. 153 (2006) A179–A186.
[23] M. Xiao, S. Choe, J. Power Sources 218 (2012) 357–367.
[24] T. Ohzuku, N. Matoba, K. Sawai, J. Power Sources 73 (2001) 97–98.
[25] L.J. Hardwick, V.A. Sethuraman, V. Srinivasan, R. Kostecki, 1st Intl. Conf. on Adv. Lithium Batteries for Automobile Applications, Argonne National Laboratory, Argonne, IL, 2008.
[26] R. Kostecki, F. McLarnon, J. Power Sources 119 (2003) 550–554.
[27] Q. Horn, K. White, Meeting of The Electrochemical Society, May 6–10 (2007).